(e, 2e) simple ionization of H_3^+ by fast electron impact: use of triangular three-center continuum and bound state wave functions

2017 J. Phys. B: At. Mol. Opt. Phys. 50 145201

(http://iopscience.iop.org/0953-4075/50/14/145201)

IOP Publishing Journal of Physics B: Atomic, Molecular and Optical Physics
J. Phys. B: At. Mol. Opt. Phys. **50** (2017) 145201 (9pp) https://doi.org/10.1088/1361-6455/aa75fa

(e, 2e) simple ionization of H_3^+ by fast electron impact: use of triangular three-center continuum and bound state wave functions

S Obeid[1], O Chuluunbaatar[2] and B B Joulakian[1,3]

[1] Université de Lorraine, SRSMC (UMR CNRS 7565), 1 bld Arago, bat. ICPM F-57078 Metz Cedex 3, France
[2] Joint Institute for Nuclear Research, Dubna, Moscow Region 141980, Russia

E-mail: boghos.joulakian@univ-lorraine.fr

Received 9 February 2017, revised 9 May 2017
Accepted for publication 31 May 2017
Published 14 June 2017

Abstract
The variation of the multiply differential cross section of the (e, 2e) simple ionization of H_3^+, with the incident and ejection energy values, as well as the directions of the ejected and scattered electrons, is studied. The calculations have been performed in the frame of the perturbative first Born procedure, which has required the development of equilateral triangular three center bound and continuum state wave functions. The results explore the optimal conditions and the particularities of the triangular targets, such as the appearance of interference patterns in the variation of the four fold differential cross section (FDCS) with the scattering angle for a fixed orientation of the molecule. The comparison between the results obtained by two H_3^+ ground wave functions, with and without a correlation term r_{12}, shows that the effect of correlation on the magnitude of the triple differential cross section is not large, but it produces some modification in the structure of the FDCS.

Keywords: e, 2e ionization, H_3^+, three center continuum wave function, electron molecule collision

(Some figures may appear in colour only in the online journal)

1. Introduction

Hydrogen is the most abundant element in the universe. It forms the simplest triatomic ion H_3^+ in equilateral triangular form [1–3], whose electronic structure has been largely studied during different periods over the past century [4–10].

H_3^+ is the subject of many studies concerning specially the dissociative recombination with electrons [11, 12] or the observations of its vibration-rotation band [13]. H_3^+ is particularly important for the understanding of the complex magnetic and ionospheric properties of planets [14, 15]. In the domain of the interaction of radiation with matter, the time evolution of H_3^+ and its isotope D_3^+ in the presence of intense laser fields, are studied theoretically in [16, 17]. Actually, the ionization of H_3^+ is less frequently studied. In this domain, we can mention the calculations of Morrison *et al* [18], who applied the spline methods to the problem of the excitation of H_3^+ to the continuum by an electromagnetic field. Also, the coincidence detection measurements, presented in [19], where the cross sections of the dissociation by multi-photon simple and double ionization of D_3^+ are measured for given orientations of the molecular plane. This is realized by the coincidence detection technique of the emerging fragments (electrons and the D_3^+ centers).

To our knowledge, the simple (e, 2e) ionization by electron impact, which consists in coincidence detection of the ejected and the scattered electrons emerging from a mono-collision of an electron with a molecular gas [20–22], has not been realized on H_3^+ yet. We have in the past developed [23] a two center continuum wave function describing the ejected

[3] Author to whom any correspondence should be addressed.

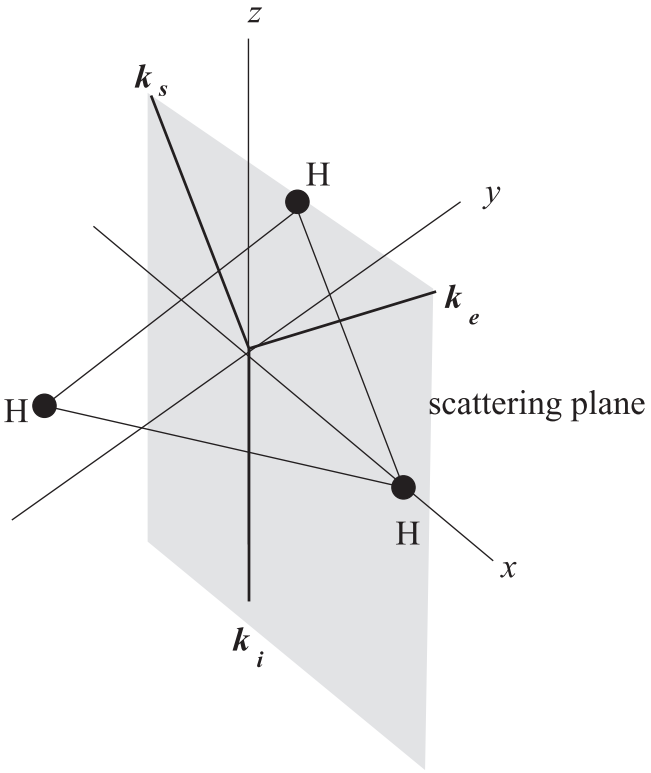

Figure 1. The collision geometry for the orientation $\alpha = \beta = \gamma = 0°$ of the molecule.

electrons from diatomic H_2^+. This model has been later applied to the (e, 2e) ionization of H_2 [24] to interpret the interference effect of a two center target. It has also been applied to the (e, 2e) of N_2 [25] and to the (e, 3e) [26] and (γ, 2e) [27, 28] double ionizations of N_2. We have later extended this model to linear three center targets and applied it to the simple and double ionizations of the $1\pi_g$, $1\pi_u$ and $3\sigma_u$ molecular orbitals of CO_2 [29–31].

The aim of the present paper is to determine the multiply differential cross section (MDCS) of the (e, 2e) process for fixed and random orientations of H_3^+ by extending the application of the three center continuum wave (ThCC) representing the slow ejected electron in the Coulomb field of the equilateral triangular potential of the residual unstable H_3^{++} dication. We present the favorable energy domains and collisional geometries to possible future measurements. Many analytic and numerical efforts were necessary for the evaluation of the MDCS. Some original aspects of these calculations are presented in the appendices.

2. Theory

Let the common origin O of the laboratory and the body fixed frame of reference be placed on the circumcenter of the equilateral triangle of H_3^+ of side ρ (see figure 1). We choose the positions of the three protons by the vectors $\mathbf{a} = \frac{\rho}{\sqrt{3}}\left(-\frac{1}{2}, +\frac{\sqrt{3}}{2}, 0\right)$, $\mathbf{b} = \frac{\rho}{\sqrt{3}}\left(-\frac{1}{2}, -\frac{\sqrt{3}}{2}, 0\right)$ and $\mathbf{c} = \frac{\rho}{\sqrt{3}}(1, 0, 0)$ defined by their body fixed cartesian coordinates.

The orientation of the molecule with respect to the laboratory frame will be given by the Euler angles α, β and γ. The MDCS of a general out-of-plane detection of the scattered and ejected electrons in the case of an oriented triatomic H_3^+ target is fourfold. It is given by

$$\sigma^{(4)}(\boldsymbol{\alpha}, \boldsymbol{\beta}, \boldsymbol{\gamma}) = \frac{\mathrm{d}^4}{\mathrm{d}\Omega_{\boldsymbol{\alpha},\boldsymbol{\beta},\boldsymbol{\gamma}}\mathrm{d}\Omega_\mathrm{s}\mathrm{d}\Omega_\mathrm{e}\mathrm{d}E_\mathrm{e}} = \frac{k_\mathrm{s}k_\mathrm{e}}{k_\mathrm{i}}|T_\mathrm{fi}|^2, \quad (1)$$

where $\mathrm{d}\Omega_\mathrm{s}$, $\mathrm{d}\Omega_\mathrm{e}$ are, respectively, the elements of the solid angles for the orientations of the scattered and the ejected electrons. $\mathrm{d}\Omega_{\boldsymbol{\alpha},\boldsymbol{\beta},\boldsymbol{\gamma}}$ represents the element of the solid Euler angles for a given orientation of the H_3^+ plane. k_i, k_s and k_e represent, respectively, the moduli of the wave vectors of the incident, scattered and ejected electrons.

In the case of randomly oriented targets, we must pass to the triple differential cross section (TDCS) by integrating over all possible and equally probable orientations of the molecule

$$\sigma^{(3)} = \frac{1}{8\pi^2}\int_0^{2\pi}\mathrm{d}\alpha\int_0^{\pi}\mathrm{d}\beta\sin(\beta)\int_0^{2\pi}\mathrm{d}\gamma\sigma^{(4)}(\alpha, \beta, \boldsymbol{\gamma}). \quad (2)$$

Using the symmetry properties of the equilateral triangle, we can show that

$$\begin{aligned}\sigma^4(\alpha, \beta, \gamma) &= \sigma^4(2\pi - \alpha, \beta, 2\pi - \gamma)\\ &= \sigma^4(\pi - \alpha, \pi - \beta, \gamma). \end{aligned} \quad (3)$$

and

$$\sigma^4(\alpha, \beta, \gamma) = \sigma^4\left(\alpha, \beta, \gamma + \frac{2\pi}{3}\right) = \sigma^4\left(\alpha, \beta, \gamma + \frac{4\pi}{3}\right). \quad (4)$$

This will reduce the limits of integration on $\boldsymbol{\alpha}$, $\boldsymbol{\beta}$ and $\boldsymbol{\gamma}$. Thus, we obtain

$$\sigma^{(3)} = \frac{3}{2\pi^2}\int_0^{\pi}\mathrm{d}\alpha\int_0^{\pi/2}\mathrm{d}\beta\sin(\beta)\int_0^{2\pi/3}\mathrm{d}\gamma\sigma^{(4)}(\boldsymbol{\alpha}, \boldsymbol{\beta}, \boldsymbol{\gamma}). \quad (5)$$

The conservation of the energy is given by

$$E_\mathrm{i} = E_\mathrm{s} + E_\mathrm{e} + I, \quad (6)$$

where E_i, E_s and E_e represent, respectively, the energy values of the incident, scattered and ejected electrons. I gives the energy necessary to eject an electron from the H_3^+ target for the equilibrium internuclear distance $\rho = 1.65$ au. The ionization process, which is much more rapid than the ro-vibrational effects, can be seen as a vertical transition from the ground state of H_3^+ at the equilibrium internuclear to the dissociative ground state of H_3^{++} at the same internuclear distance. The separation of the rotational and vibrational levels, which cannot be resolved in the actual (e, 2e) experiments, can be done by applying the closure relations over these levels. This is explained by Iijima *et al* [32] in the case of electron scattering from diatomic targets.

The transition matrix element T_fi, the square modulus of which is proportional to the probability of a particular event, is a combination of three terms corresponding to the possible quantum exchanges between the incident and the two bound electrons, given by Shulz [33] after having taken into

account the spin combination of the incident and the bound electrons for the case of two electron targets. These terms are, the direct term and the two exchange terms. In the direct term, given below, the incident electron is supposed to become the scattered in the final state. The first exchange term corresponds to the transition in which the incident electron and the ejected electron are supposed to be the same, and finally the capture term or the exchange of the second type, for which the incident electron and the final state bound electron are supposed to be the same (see [33]). In the relatively high incident electron energy domain (>500 eV) that we will explore, the contributions of the two last exchange terms are negligible, with respect to the direct term [33], which is given by

$$T_{\rm fi} = \frac{\sqrt{2}}{2\pi}\int \mathbf{dR}\int \mathbf{dr}_1\int \mathbf{dr}_2 \exp(\imath \mathbf{KR}) \times \Psi_{\rm i}(\mathbf{r}_1, \mathbf{r}_2) V(\mathbf{R}, \mathbf{r}_1, \mathbf{r}_2)\overline{\Psi}_f(\mathbf{r}_1, \mathbf{r}_2). \quad (7)$$

Here, the bar indicates the complex conjugate. $\mathbf{R}$ is the position of the fast incident (scattered) electron, which we will describe by plane waves having, respectively, the wave vectors $\mathbf{k}_{\rm i}$ and $\mathbf{k}_{\rm s}$. These two vectors define the scattering plane (see figure 1). The z axis of the laboratory frame is parallel to $\mathbf{k}_{\rm i}$. $\mathbf{r}_1$, $\mathbf{r}_2$ refer to the positions of the target electrons. $\mathbf{K} = \mathbf{k}_{\rm i} - \mathbf{k}_{\rm s}$ is the momentum transferred to the target. and $V(\mathbf{R}, \mathbf{r}_1, \mathbf{r}_2)$ represents the Coulomb interaction between the incident electron and the target given by

$$V(\mathbf{R}, \mathbf{r}_1, \mathbf{r}_2) = \frac{1}{|\mathbf{R} - \mathbf{r}_1|} + \frac{1}{|\mathbf{R} - \mathbf{r}_2|} - \frac{1}{|\mathbf{R} - \mathbf{a}|} - \frac{1}{|\mathbf{R} - \mathbf{b}|} - \frac{1}{|\mathbf{R} - \mathbf{c}|}. \quad (8)$$

Using the Bethe transformation for the position vector $\mathbf{R}$ of the incident fast electron in equation (7)

$$\int \mathbf{dR}\frac{\exp(\imath \mathbf{KR})}{|\mathbf{R} - \mathbf{r}|} = 4\pi\frac{\exp(\imath \mathbf{Kr})}{K^2}, \quad (9)$$

the transition matrix element $T_{\rm fi}$ will be reduced to

$$T_{\rm fi} = \frac{2\sqrt{2}}{K^2}\int \mathbf{dr}_1\int \mathbf{dr}_2 \Psi_{\rm i}(\mathbf{r}_1, \mathbf{r}_2) U(\mathbf{r}_1, \mathbf{r}_2)\bar{\Psi}_f(\mathbf{r}_1, \mathbf{r}_2), \quad (10)$$

$$U(\mathbf{r}_1, \mathbf{r}_2) = \exp(\imath \mathbf{Kr}_1) + \exp(\imath \mathbf{Kr}_2) - \exp(\imath \mathbf{Ka}) - \exp(\imath \mathbf{Kb}) - \exp(\imath \mathbf{Kc}). \quad (11)$$

2.1. The initial state wave function

For the initial state wave function $\Psi_i(\mathbf{r}_1, \mathbf{r}_2) \equiv \Psi_{H_3^+}(\mathbf{r}_1, \mathbf{r}_2)$ of H_3^+ molecular ion at the equilibrium internuclear distance $\rho = 1.65$ au, we choose the following solution

$$\Psi_{H_3^+}(\mathbf{r}_1, \mathbf{r}_2) = N_{H_3^+}(1 + P_{12}) \times \sum_{\rm perm\{a,b,c\}} \exp(-\alpha_1 r_{1a} - \alpha_2 r_{1b} - \alpha_3 r_{1c} - \alpha_4 r_{2a} - \alpha_5 r_{2b} - \alpha_6 r_{2c} + \alpha_7 r_{12}), \quad (12)$$

where

$$\mathbf{r}_{12} = \mathbf{r}_1 - \mathbf{r}_2, \quad \mathbf{r}_{ja} = \mathbf{r}_j - \mathbf{a}, \quad \mathbf{r}_{jb} = \mathbf{r}_j - \mathbf{b}. \quad \mathbf{r}_{jc} = \mathbf{r}_j - \mathbf{c}, \quad j = 1, 2, \quad (13)$$

P_{12} and perm$\{a, b, c\}$ are, respectively, the operators that permute electrons ($1 \leftrightarrow 2$) and the three nuclei ($\mathbf{a} \leftrightarrow \mathbf{b} \leftrightarrow \mathbf{c}$). In table 1 we present the numerical values of the parameters for two functions. The first function corresponds to the one that we determined with 6 variational parameters and the second one with seven parameters, in which r_{12} is present. To our knowledge, this function, which is constructed, for each electron, by a product of three exponential functions, each related to one of the nuclei ($\mathbf{a}$, $\mathbf{b}$, $\mathbf{c}$) was first given in [34]. They insure more rapid convergence in the determination of the integrals than ordinary LCAO type functions. A similar function was first employed for the diatomic case in [35] and then in [36].

In appendices A–C we present some basic details for the determination of the mono and bi-electronic integrals, that we have met in the determination of this function by the variational method. We observe that, the introduction of the r_{12} correlation term ($\alpha_7 \neq 0$) in the second function improves the energy ($E_{H_3^+} = -1.331\,48$ to $E_{H_3^+} = -1.340\,34$ au). Here we must mention that, the best total energy value $E_{H_3^+} = -1.343\,835\,625\,02$ au is obtained by a trial wave function containing 1000 explicitly correlated spherical Gaussian terms [37], whose application in our calculation of the MDCS would need very long and cumbersome computational efforts, which is not realistic at this stage.

2.2. The final state wave function

Following [33], the final state wave function in the direct term equation (10), describing the state of the ejected and bound electrons is written by the following product

$$\Psi_f(\mathbf{r}_1, \mathbf{r}_2) = \Psi_c(\mathbf{k}_{\rm e}, \mathbf{r}_1)\Psi_{H_3^{++}}(\mathbf{r}_2). \quad (14)$$

Here $\Psi_{H_3^{++}}(\mathbf{r})$ and $\Psi_c(\mathbf{k}_{\rm e}, \mathbf{r})$ are, respectively, the discrete and continuum state wave functions of the residual H_3^{++} molecular ion and the ejected electron. As mentioned above, the ionization process is considered as a vertical transition, so for these functions $\rho = 1.65$ au, the equilibrium distance of the target H_3^+. For the present work we have made the choice to apply for the bound electron, the following simple, but quite satisfactory wave function

$$\Psi_{H_3^{++}}(\mathbf{r}) = N_{H_3^{++}} \sum_{\rm perm\{a,b,c\}} \exp(-\beta_1 r_a - \beta_2 r_b - \beta_3 r_c), \quad (15)$$

that we determined with our variational procedure. It gives the total energy value $E_{H_3^{++}} = -0.111\,46$ au (table 2). In appendices A and B we present some details of our approach in the determination of the needed matrix elements. We must mention here, that a similar wave function, but with 14 parameters and 25 exponential terms is available in [38]. It results in a total energy value of $E_{H_3^{++}} = -0.111860\,55$ au.

As mentioned above, the originality of the present paper is also in the introduction, for the first time, of the three center

Table 1. The ground state energy, the norm and the variational parameters of the wave function equation (12) at the equilibrium internuclear distance $\rho = 1.65$ au of H_3^+.

	$E_{H_3^+}$ (au)	$N_{H_3^+}$	α_1	α_2	α_3	α_4	α_5	α_6	α_7
Present	−1.331 48	0.17628	−0.43129	0.35127	1.38683	1.09057	0.24560	0.39686	0.00000
[34]	−1.34034	0.22115	−0.00353	0.18548	1.42450	1.04710	0.15082	0.58912	0.21632
[37]	−1.343 835 625 02								

Table 2. The total energy, the norm and the variational parameters of the wave function equation (15) for $\rho = 1.65$ au of H_3^{++}.

	$E_{H_3^{++}}$ (au)	$N_{H_3^{++}}$	β_1	β_2	β_3
Present	−0.111 46	0.35121	1.28963	0.11826	0.32445
[38]	−0.111 860 55				

description of the ejected electron in the field of H_3^{++}, inspired from [29]:

$$\Psi_c(\mathbf{k}, \mathbf{r}) = M\frac{\exp(\imath\mathbf{kr})}{(2\pi)^{3/2}}\prod_{j=a,b,c} {}_1F_1(\imath\xi, 1, -\imath(kr_j + \mathbf{kr}_j)),$$
$$M = \left(\exp\left(-\pi\frac{\xi}{2}\right)\Gamma(1 - \imath\xi)\right)^3, \quad \xi = -\frac{2}{3}\frac{1}{k}. \tag{16}$$

The advantage of this function, compared to one center models applied habitually to molecules, is that it satisfies the exact asymptotic conditions and possesses, by its nature, the triangular symmetry of the target

$$\lim_{r\to\infty}\Psi_c(\mathbf{k}, \mathbf{r}) \longrightarrow \frac{\exp(\imath\mathbf{kr})}{(2\pi)^{3/2}}\exp(-\imath 3\xi\ln(kr + \mathbf{kr})). \tag{17}$$

The interaction between the ejected electron and the electron cloud of the H_3^{++} ion is taken into account here through the $\xi = -\frac{2}{3}\frac{1}{k}$, which gives the real global charge of 2 'seen' by the ejected electron. This could be enough only for ejected electrons with moderate energies values around 30 eV. We are conscious that, for slower ejected electrons, the introduction of the polarization of the electron cloud of the residual ion H_3^{++}, which could brake the C_{3v} symmetry, and eventually the second term of the Born series of the transition matrix element, could have important effects. We have the intention to introduce these effects in our future calculations.

3. Results and discussion

As we mentioned in the introduction, the aim of this paper is to study the variation of the multiply differential cross sections of the complete (e, 2e) experiment on H_3^+ for typical geometries, that can be realized in the near future. In fact, coincidence detection measurements are already realized in multi-photon dissociation and simple and double ionization of oriented and randomly oriented D_3^+ targets [19]. We will try here, to extract to optimal experimental conditions, which result in satisfactory number of counts of coincidence events and analyze the electronic structure of the target and the mechanisms of the ionization.

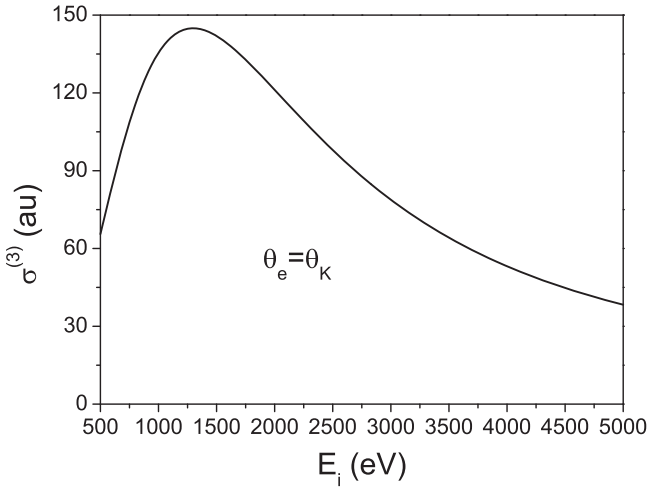

Figure 2. The variation of the TDCS of the (e, 2e) simple ionization of H_3^+ with the incident energy E_i. The energy of the ejected electron $E_e = 10$ eV. The scattering angle $\theta_s = -1°$. The direction of the ejected electron is parallel to the momentum transfer $\theta_e = \theta_K$. The full line corresponds to the results obtained by the correlated initial state wave function (12) with $\alpha_7 \neq 0$. The dashed line, to those obtained by the non-correlated initial state wave function (12) with $\alpha_7 = 0$.

We begin first by the variation of the TDCS given by equation (5) with the incident energy E_i. The wave vectors $\mathbf{k}_i$ and $\mathbf{k}_s$ define the collision plane. We chose the z axis of the laboratory frame parallel to $\mathbf{k}_i$. We fix the ejection energy $E_e = 10$ eV and the ejection direction parallel to the momentum transfer. The angle of the scattered electron with the incidence direction $\theta_s = -1°$. The results of our calculations obtained by the application of both correlated and less correlated wave functions are shown in figure 2. Both results show that, for the random orientation of the target, the value of the incident electron which gives the higher values of the TDCS is around $E_i \approx 1300$ eV. The small difference in magnitude of the two curves shows that the introduction of more electron-electron correlation between the bound electrons by the introduction of $\alpha_7 \neq 0$ has little effect on the simple ionization process, which is mostly caused by the

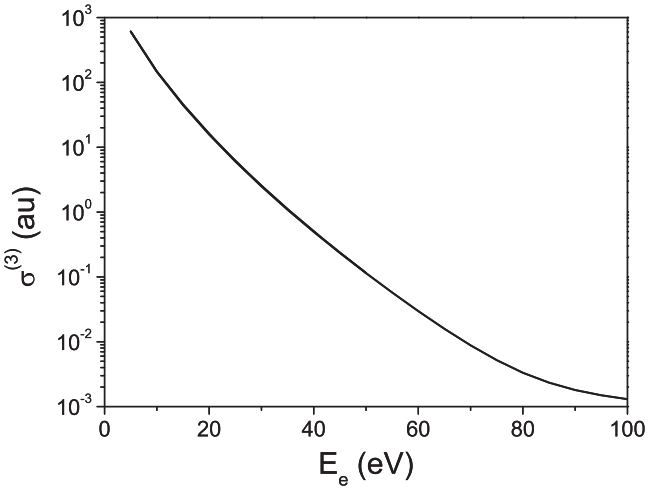

Figure 3. The variation of the TDCS with the ejected energy E_e. The energy of the incident electron $E_i = 1300$ eV. The other conditions are similar to that of figure 2.

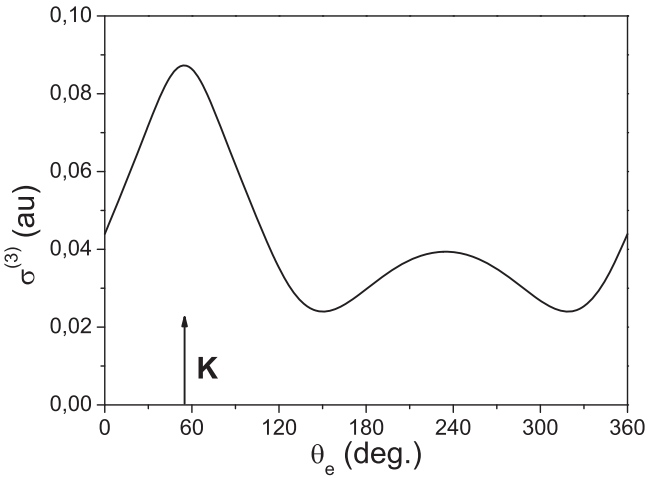

Figure 4. The variation of the TDCS in terms of the ejection angle θ_e. The energy of the scattered electron $E_s = 500$ eV, which is detected at an angle $\theta_s = -6°$ in coincidence with the ejected electron with energy $E_e = 37$ eV. The results are obtained by the correlated initial state wave function (12) with $\alpha_7 \neq 0$.

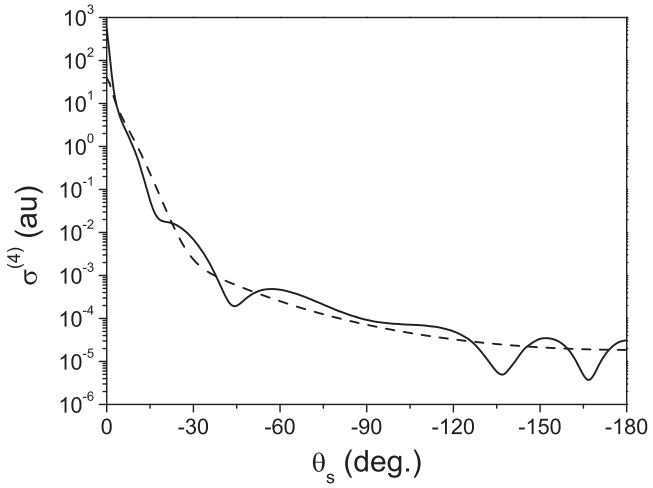

Figure 5. The variation of the FDCS in terms of the scattering angle θ_s, with the molecular plane perpendicular to $\mathbf{k}_i$, i.e. $\alpha = 0°$, $\beta = 0°$ and $\gamma = 0°$. The incident energy is $E_i = 1300$ eV. The ejected electron with $E_e = 10$ eV emerges in the direction of the momentum transfer $\theta_e = \theta_K$. The full line represents the results obtained with the correlated initial state wave function with $\alpha_7 \neq 0$ equation (12). The dashed line gives the results for the ionization of Li^+ target in the same conditions.

exchange of energy and momentum between the incident and the ejected electron.

We then pass to the variation of the TDCS with the ejection energy, by considering the 'best' incident energy $E_i = 1300$ eV obtained above, and keeping the same ejection and scattering directions. We mentioned above that our procedure does not take into account the polarization of the electron cloud of the residual ion, and that, the ThCC wave function equation (16) would not be well adapted for very slow ejected electrons. In spite of this, we made the choice to begin our exploration with $E_e = 5$ eV and go up to 100 eV, knowing that for lower values of the energy, the results should be considered as preliminary indications. We observe in figure 3, that the TDCS decreases continuously. This can be due to the fact that the scattering angle, being relatively small $\theta_s = -1°$, the modulus of the momentum transferred to the target is also small, the ejected electron has less of a chance to acquire high kinetic energy values.

In figure 4, we pass to the variation of the TDCS with the ejection angle θ_e. In this case, we chose the experimental conditions of the (e, 2e) set up of the University of Orsay [25]. Here the energy of the scattered electron $E_s = 500$ eV detected at an angle $\theta_s = -6°$ in coincidence with the ejected electron energy $E_e = 37$ eV. We observe that the position of the first maximum around $\theta_e = 60°$ which corresponds to the ejection direction parallel to the momentum transfer is respected. The second maximum around $\theta_e = 240°$ corresponds to the recoil peak. This shows that when one considers random orientations of the target, the semi-classical analysis for which, these two directions are favorable ejection directions of the (e, 2e) process are also true for the triatomic targets.

Let us pass to a situation where the molecule has a fixed orientation. This can be observed experimentally by detecting the emerging nuclei in coincidence with the electrons for the desired orientation [19]. We begin first by the variation of the four fold differential cross section (FDCS) equation (1) with the scattering angle θ_s. This is shown in figure 5. Here the molecular plane is kept perpendicular to the incident direction ($\alpha = 0°$, $\beta = 0°$ and $\gamma = 0°$). As θ_s varies between 0° and 180° degrees, we observe interference patterns due to the three centers of the target, which should play the role of obstacles, by analogy to optical interference set ups. These patterns should depend on the separation of the three nuclei given by ρ and, thus, be a characteristic of a given molecule. To verify this, we repeated, in the same conditions, the calculation for the Li^+ target, which can be consider

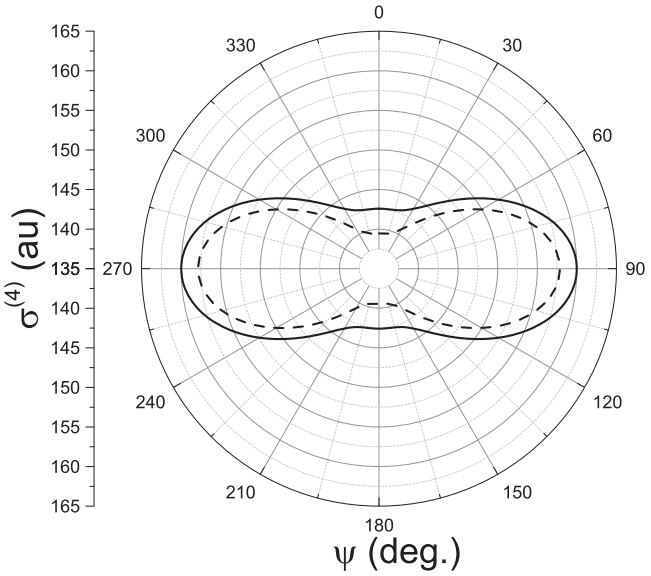

Figure 6. Variation of the FDCS in polar representation, where the radius represents the magnitude of the FDCS and the polar angle ψ represents the rotation around the x axis of the laboratory frame. Initially $\alpha = 0°$, $\beta = 0°$ and $\gamma = 0°$. Here the incident energy is $E_i = 1300$ eV, with the scattered angle $\theta_s = -1°$ and the energy of the ejected electron is $E_e = 10$ eV, whose direction is parallel to the momentum transfer $\theta_e = \theta_K$. The full line represents the results obtained by the correlated initial state wave function (12) with $\alpha_7 \neq 0$, and the dashed line represents those obtained by the non-correlated initial state wave function (12) with $\alpha_7 = 0$.

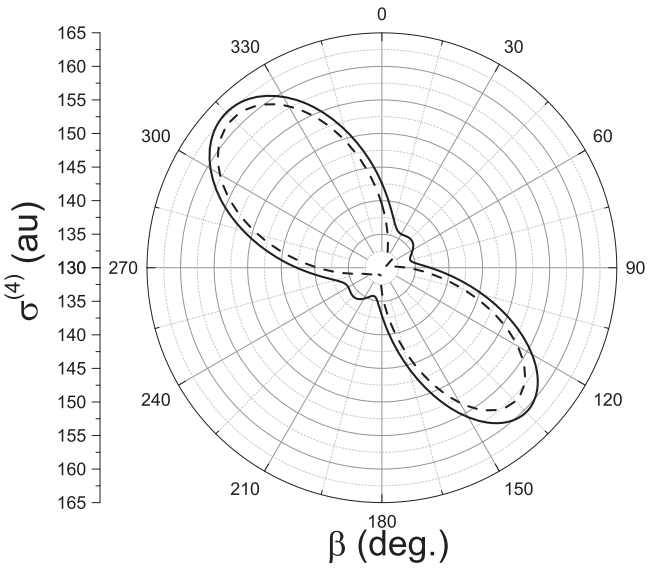

Figure 7. The same as in figure 6, but for rotations around the y axis with the angle β.

as the united atom limit of H_3^+ . We observe that, as expected, the interference pattern disappears as the triangular target becomes a united atom.

In the following three cases we will rotate the molecule around each of the three axes Ox, Oy and Oz. The results are shown in figures 6–8, respectively. They show the variations of the FDCS in polar representation ,where the polar angles

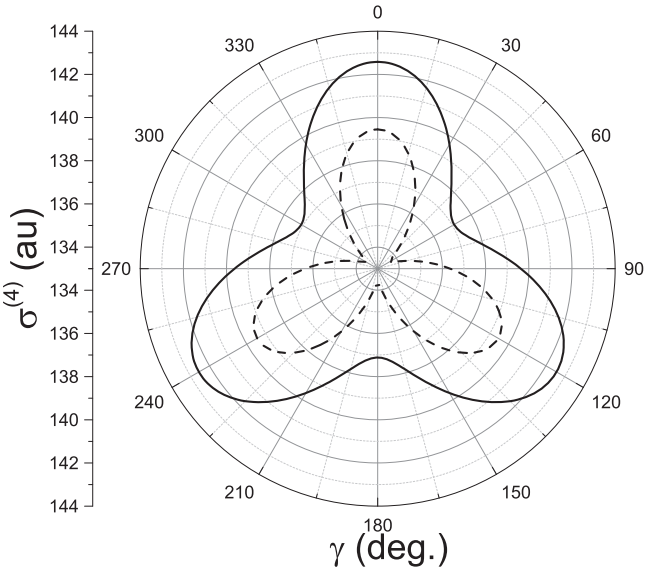

Figure 8. The same as in figure 6, but for the rotation around the z axis with angle γ.

representing the angle of rotation of the molecule beginning always from the initial orientation $\alpha = 0°$, $\beta = 0°$ and $\gamma = 0°$ as shown in figure 1. The magnitude of the FDCS is represented by the radius of a given point on the curve. We recall that the direction of the incident electron is always parallel to the z axis of the laboratory.

In the first case, we observe in figure 6 that the structure of the curve is symmetrical around the line going from $\psi = 0°$ to $\psi = 180°$ and that going from $\psi = 90°$ to $\psi = 270°$. The FDCS being maximal when $\psi = 90°$ or $\psi = 270°$, which correspond to the situations for which the plane of the molecule coincides with the collision plane formed by the vectors $\mathbf{k}_i$ and $\mathbf{k}_s$. This can be explained by the fact that, for these two orientations of the molecule, the electron cloud of the target H_3^+ from which the ejected electron will emerge is parallel to the incident electronic flux. Now comparing the two curves corresponding to the two initial state wave functions we observe some small but perceptible differences in magnitude and structure which, as we mentioned for figure 2, should be a manifestation of electron–electron correlation present more in the first wave function than in the second.

In figure 7, we show in the same manner as in figure 6, the variation of the FDCS for the rotation of the molecule around the y axis, which we recall is perpendicular to the two parallel vectors $\mathbf{k}_e$ and $\mathbf{K}$. Here the angle of rotation is given by β. To analyze the particularities of the structure of this curve, we must precise, that here $\theta_K = 45°$ for this particular geometry. Now when $\beta = 45°$ or $\beta = 225°$ the molecular plane will include the vectors $\mathbf{k}_e$ and $\mathbf{K}$. When $\beta = 135°$ and $\beta = 315°$ the vectors $\mathbf{k}_e$ and $\mathbf{K}$ will be perpendicular to the molecular plane. These are favorable orientations because the recoil momentum of the molecule is perpendicular to the molecular plane. We also observe that the symmetry condition $\sigma^4\left(0, \frac{3\pi}{4} + \phi, 0\right) = \sigma^4\left(0, \frac{3\pi}{4} - \phi, 0\right)$ deduced by direct Euler angle transformation properties, is respected in our result.

We then pass to the rotation around Oz axis shown in figure 8. Here $\alpha = 0°$ and $\beta = 0°$ and the rotation angle is represented by γ. Here also the the results of the calculation confirm the expected symmetry inherent to the triangular symmetry of the target. the three maxima of the curves correspond to equivalent orientations of the molecule.

4. Conclusion

We have determined the MDCS of the (e, 2e) simple ionization of H_3^+ by employing perturbative first Born procedure and the three center continuum wave function adapted to the equilateral triangular case. We have explored the influence of the initial state electron–electron correlation, determined some favorable conditions and shown the particularities of the triangular targets, specially the interference patterns in the variation of the four fold differential for fixed orientation of the molecular plane FDCS with the scattering angle. Our calculations could be considered as exploratory in advance of experimental results. We hope to introduce the polarization effect of the residual ion H_3^{++} which is absent in the present procedure in our future calculations.

Acknowledgments

OC acknowledges support from the Hulubei-Meshcheryakov program JINR-Romania. Most of the calculations were performed on Central Information and Computer Complex, and HybriLIT heterogeneous computing cluster of the Joint Institute for Nuclear Research.

Appendix A. Determination of the three center basic mono-electronic integral

Let us consider the three-dimensional integral

$$J(\zeta, \eta, \xi) = \int \mathrm{d}\mathbf{r} \frac{\exp(-\zeta r_a)}{r_a} \frac{\exp(-\eta r_b)}{r_b} \frac{\exp(-\xi r_c)}{r_c},$$
$$\mathbf{r}_a = \mathbf{r} - \mathbf{a}, \quad \mathbf{r}_b = \mathbf{r} - \mathbf{b}, \quad \mathbf{r}_c = \mathbf{r} - \mathbf{c}, \quad \zeta, \eta, \xi > 0. \tag{A.1}$$

During the numerical determination of this three center integral, one must be very cautious to the singularities. Here we present our approach to avoid the singular points. We begin by replacing the following Fourier transform in the above integral

$$\Psi(\mathbf{r}) = \frac{\exp(-\xi r)}{r} = \frac{4\pi}{(2\pi)^3} \int \mathrm{d}\mathbf{p} \frac{\exp(\imath \mathbf{p}\mathbf{r})}{\xi^2 + p^2}, \tag{A.2}$$

which becomes

$$\begin{aligned} J(\zeta, \eta, \xi) &= \frac{(4\pi)^2}{(2\pi)^6} \int \mathrm{d}\mathbf{p} \int \mathrm{d}\mathbf{q} \int \mathrm{d}\mathbf{r} \frac{\exp(\imath \mathbf{p}(\mathbf{r} - \mathbf{a}))}{\zeta^2 + p^2} \\ &\times \frac{\exp(\imath \mathbf{q}(\mathbf{r} - \mathbf{b}))}{\eta^2 + q^2} \frac{\exp(-\xi r_c)}{r_c} \\ &= \frac{(4\pi)^2}{(2\pi)^6} \int \mathrm{d}\mathbf{p} \frac{\exp(\imath \mathbf{p}(\mathbf{c} - \mathbf{a}))}{\zeta^2 + p^2} \\ &\times \int \mathrm{d}\mathbf{q} \frac{\exp(\imath \mathbf{q}(\mathbf{c} - \mathbf{b}))}{\eta^2 + q^2} \\ &\times \int \mathrm{d}\mathbf{r}_c \frac{\exp(-\xi r_c + \imath(\mathbf{p} + \mathbf{q})\mathbf{r}_c)}{r_c} \\ &= \frac{(4\pi)^3}{(2\pi)^6} \int \mathrm{d}\mathbf{p} \frac{\exp(\imath \mathbf{p}(\mathbf{c} - \mathbf{a}))}{\zeta^2 + p^2} \int \mathrm{d}\mathbf{q} \\ &\times \frac{\exp(\imath \mathbf{q}(\mathbf{c} - \mathbf{b}))}{(\eta^2 + q^2)(\xi^2 + (\mathbf{p} + \mathbf{q})^2)}. \end{aligned} \tag{A.3}$$

We then use the following relation

$$\frac{1}{(\eta^2 + q^2)(\zeta^2 + (\mathbf{q} + \mathbf{p})^2)} = \int_0^1 \frac{\mathrm{d}x}{(\mu^2 + (\mathbf{q} + x\mathbf{p})^2)^2},$$
$$\mu^2 = x(1 - x)p^2 + (1 - x)\eta^2 + x\zeta^2, \tag{A.4}$$

and integrate over $\mathbf{q}$

$$\begin{aligned} &\int \mathrm{d}\mathbf{q} \frac{\exp(\imath \mathbf{q}(\mathbf{c} - \mathbf{b}))}{(\eta^2 + q^2)(\xi^2 + (\mathbf{p} + \mathbf{q})^2)} \\ &= \int_0^1 \mathrm{d}x \exp(-\imath x \mathbf{p}(\mathbf{c} - \mathbf{b})) \int \mathrm{d}\mathbf{q} \frac{\exp(\imath(\mathbf{q} + x\mathbf{p})(\mathbf{c} - \mathbf{b}))}{(\mu^2 + (\mathbf{q} + x\mathbf{p})^2)^2} \\ &= \pi^2 \int_0^1 \mathrm{d}x \exp(-\imath x \mathbf{p}(\mathbf{c} - \mathbf{b})) \frac{\exp(-\mu|\mathbf{c} - \mathbf{b}|)}{\mu}. \end{aligned} \tag{A.5}$$

Finally, the three-dimensional basic integral (A.3) takes the following form, which presents the advantage of avoiding the singular points

$$\begin{aligned} J(\zeta, \eta, \xi) &= \frac{(4\pi)^3 \pi^2}{(2\pi)^6} \int \mathrm{d}\mathbf{p} \int_0^1 \mathrm{d}x \\ &\times \frac{\exp(\imath \mathbf{p}[(\mathbf{c} - \mathbf{a}) - x(\mathbf{c} - \mathbf{b})])}{\zeta^2 + p^2} \frac{\exp(-\mu|\mathbf{c} - \mathbf{b}|)}{\mu} \\ &= 4 \int_0^\infty \mathrm{d}p \int_0^1 \mathrm{d}x \frac{p}{\zeta^2 + p^2} \\ &\times \frac{\sin(p|(\mathbf{c} - \mathbf{a}) - x(\mathbf{c} - \mathbf{b})|)}{|(\mathbf{c} - \mathbf{a}) - x(\mathbf{c} - \mathbf{b})|} \frac{\exp(-\mu|\mathbf{c} - \mathbf{b}|)}{\mu}. \end{aligned} \tag{A.6}$$

Appendix B. Determination of the three center mono-electronic matrix elements

We begin with the relations

$$\nabla_{\mathbf{r}}\exp(-\zeta r) = -\zeta\frac{\mathbf{r}}{r}\exp(-\zeta r),$$
$$2\mathbf{r}_a\mathbf{r}_b = r_a^2 + r_b^2 - (\mathbf{b}-\mathbf{a})^2, \quad 2\mathbf{r}_a\mathbf{r}_c = r_a^2 + r_c^2 - (\mathbf{c}-\mathbf{a})^2,$$
$$2\mathbf{r}_b\mathbf{r}_c = r_b^2 + r_c^2 - (\mathbf{c}-\mathbf{b})^2. \tag{B.1}$$

We define then

$$J_{nlm}(\zeta,\eta,\xi) = (-1)^{n+l+m}\frac{\partial^{n+l+m}J(\zeta,\eta,\xi)}{\partial\zeta^n\partial\eta^l\partial\xi^m}. \tag{B.2}$$

Letting

$$\zeta_{ij} = \zeta_i + \zeta_j, \quad \eta_{ij} = \eta_i + \eta_j, \quad \xi_{ij} = \xi_i + \xi_j,$$

we can now express the matrix elements of the mono-electronic kinetic energy, the Coulomb attraction and the normalization, respectively, in terms of combinations of J_{nlm}:

$$\begin{aligned}
K_{ij} &= -\frac{1}{2}\langle\exp(-\zeta_i r_a - \eta_i r_b - \xi_i r_c)|\Delta_{\mathbf{r}}| \\
&\quad\times\exp(-\zeta_j r_a - \eta_j r_b - \xi_j r_c)\rangle \\
&= \frac{\zeta_i\zeta_j + \eta_i\eta_j + \xi_i\xi_j}{2}J_{111}(\zeta_{ij},\eta_{ij},\xi_{ij}) \\
&\quad+\frac{\zeta_i\eta_j + \eta_i\zeta_j}{4}[J_{201}(\zeta_{ij},\eta_{ij},\xi_{ij}) + J_{021}(\zeta_{ij},\eta_{ij},\xi_{ij}) \\
&\quad-(\mathbf{b}-\mathbf{a})^2J_{001}(\zeta_{ij},\eta_{ij},\xi_{ij})] \\
&\quad+\frac{\zeta_i\xi_j + \xi_i\zeta_j}{4}[J_{210}(\zeta_{ij},\eta_{ij},\xi_{ij}) + J_{012}(\zeta_{ij},\eta_{ij},\xi_{ij}) \\
&\quad-(\mathbf{c}-\mathbf{a})^2J_{010}(\zeta_{ij},\eta_{ij},\xi_{ij})] \\
&\quad+\frac{\eta_i\xi_j + \xi_i\eta_j}{4}[J_{120}(\zeta_{ij},\eta_{ij},\xi_{ij}) + J_{102}(\zeta_{ij},\eta_{ij},\xi_{ij}) \\
&\quad-(\mathbf{c}-\mathbf{b})^2J_{100}(\zeta_{ij},\eta_{ij},\xi_{ij})], \\
P_{ij} &= -\left\langle\exp(-\zeta_i r_a - \eta_i r_b - \xi_i r_c)\left|\frac{1}{r_a}+\frac{1}{r_b}+\frac{1}{r_c}\right|\right. \\
&\quad\left.\times\exp(-\zeta_j r_a - \eta_j r_b - \xi_j r_c)\right\rangle, \\
&= -J_{011}(\zeta_{ij},\eta_{ij},\xi_{ij}) - J_{101}(\zeta_{ij},\eta_{ij},\xi_{ij}) - J_{011}(\zeta_{ij},\eta_{ij},\xi_{ij}), \\
M_{ij} &= \langle\exp(-\zeta_i r_a - \eta_i r_b - \xi_i r_c)|\exp(-\zeta_j r_a - \eta_j r_b - \xi_j r_c)\rangle \\
&= J_{111}(\zeta_{ij},\eta_{ij},\xi_{ij}).
\end{aligned} \tag{B.3}$$

Appendix C. Determination of the three center bi-electronic matrix elements

The Hamiltonian which describes the ion H_3^+ under the assumption that the protons are infinitely massive and located at the vertices of an equilateral triangle of side ρ is written as follows:

$$H = -\frac{1}{2}\sum_{i=1}^{2}\Delta_{\mathbf{r}_i} - \sum_{i=1,2}\sum_{k=a,b,c}\frac{1}{r_{jk}} + \frac{1}{r_{12}} + \frac{3}{\rho}, \tag{C.1}$$

where

$$\begin{aligned}
&\mathbf{r}_{12} = \mathbf{r}_1 - \mathbf{r}_2, \quad \mathbf{r}_{ja} = \mathbf{r}_j - \mathbf{a}, \quad \mathbf{r}_{jb} = \mathbf{r}_j - \mathbf{b}. \\
&\mathbf{r}_{jc} = \mathbf{r}_j - \mathbf{c}, \quad j = 1, 2.
\end{aligned} \tag{C.2}$$

We seek the initial state wave function $\Psi(\mathbf{r}_1, \mathbf{r}_2)$ at the equilibrium internuclear distance $\rho = 1.65$ au [34]

$$\begin{aligned}
\Psi(\mathbf{r}_1,\mathbf{r}_2) = (1+P_{12})\times\sum_{\mathrm{perm}\{a,b,c\}}&\exp(-\alpha_1 r_{1a} - \alpha_2 r_{1b} \\
&- \alpha_3 r_{1c} - \alpha_4 r_{2a} - \alpha_5 r_{2b} - \alpha_6 r_{2c} + \alpha_7 r_{12}).
\end{aligned} \tag{C.3}$$

We want to determine $E = E(\alpha_1, \alpha_2, \alpha_3, \alpha_4, \alpha_5, \alpha_6, \alpha_7)$ by minimization techniques. We have

$$\frac{\partial E}{\partial\alpha_i} = \frac{\partial}{\partial\alpha_i}\frac{\langle\Psi|H|\Psi\rangle}{\langle\Psi|\Psi\rangle} = 2\frac{\left\langle\frac{\partial\Psi}{\partial\alpha_i}|H-E|\Psi\right\rangle}{\left\langle\frac{\partial\Psi}{\partial\alpha_i}|\Psi\right\rangle}, \tag{C.4}$$

where $\frac{\partial\Psi}{\partial\alpha_i}$ can be calculated analytically.

Thus, we have to determine a six-dimensional repulsive Coulomb integral of the following form:

$$I = \int d\mathbf{r}_1\int d\mathbf{r}_2\frac{f(\mathbf{r}_1,\mathbf{r}_2)}{r_{12}}, \quad \mathbf{r}_{12} = \mathbf{r}_1 - \mathbf{r}_2. \tag{C.5}$$

To avoid singular points in the numerical determination of this type of integral we make a transformation of the angular coordinates:

$$\theta_1, \phi_1, \theta_2, \phi_2 \quad\longmapsto\quad \theta = \theta_1, \phi = \phi_1, \theta_{12}, \psi. \tag{C.6}$$

Here θ_{12} is the angle between $\mathbf{r}_1$ and $\mathbf{r}_2$, ψ is the angle between the plane defined by the vectors $(\mathbf{r}_1, \mathbf{r}_2)$ and that defined by $(\mathbf{r}_1, z)$

$$0 \leqslant \theta_{12} \leqslant \pi, \quad 0 \leqslant \psi \leqslant 2\pi. \tag{C.7}$$

In this case the unit vector $\hat{\mathbf{r}}_2 = (\hat{x}_2, \hat{y}_2, \hat{z}_2)$ of the vector $\mathbf{r}_2$ has the form

$$\begin{aligned}
\begin{pmatrix}\hat{x}_2\\ \hat{y}_2\\ \hat{z}_2\end{pmatrix} &= \begin{pmatrix}\cos(\phi_1) & -\sin(\phi_1) & 0\\ \sin(\phi_1) & \cos(\phi_1) & 0\\ 0 & 0 & 1\end{pmatrix}\begin{pmatrix}\cos(\theta_1) & 0 & \sin(\theta_1)\\ 0 & 1 & 0\\ -\sin(\theta_1) & 0 & \cos(\theta_1)\end{pmatrix} \\
&\quad\times\begin{pmatrix}\sin(\theta_{12})\cos(\pi-\psi)\\ \sin(\theta_{12})\sin(\pi-\psi)\\ \cos(\theta_{12})\end{pmatrix}.
\end{aligned} \tag{C.8}$$

The integral (C.5) is, thus, transformed to

$$\begin{aligned}
I = &\int_0^\infty dr_1 r_1^2\int_0^\infty dr_2 r_2^2\int_0^\pi d\theta_1\sin(\theta_1)\int_0^{2\pi}d\phi_1 \\
&\times\int_0^{2\pi}d\psi\int_0^\pi d\theta_{12}\sin(\theta_{12})\frac{f(\mathbf{r}_1,\mathbf{r}_2)}{\sqrt{r_1^2 + r_2^2 - 2r_1r_2\cos(\theta_{12})}}.
\end{aligned} \tag{C.9}$$

Applying the following change of variables

$$r_1 = r\sin(\alpha/2), \quad r_2 = r\cos(\alpha/2), \quad 0 \leqslant r < \infty, \quad 0 \leqslant \alpha \leqslant \pi. \tag{C.10}$$

The integral becomes

$$I = \frac{1}{8}\int_0^\infty \mathrm{d}r r^4 \int_0^\pi \mathrm{d}\alpha \sin^2(\alpha)\int_0^\pi \mathrm{d}\theta_1 \sin(\theta_1)\int_0^{2\pi}\mathrm{d}\phi_1 \times \int_0^{2\pi}\mathrm{d}\psi \int_0^\pi \mathrm{d}\theta_{12}\sin(\theta_{12})\frac{f(\mathbf{r}_1,\mathbf{r}_2)}{\sqrt{1-\sin(\alpha)\cos(\theta_{12})}}. \tag{C.11}$$

Now using the change of variable θ_{12} used in [39] we have

$$\cos(\theta_{12}) = \begin{cases} (1-\xi^2)\frac{\tan(\alpha/2)}{2} + \xi, & 0 \leqslant \alpha \leqslant \pi/2, \\ (1-\xi^2)\frac{\cot(\alpha/2)}{2} + \xi, & \pi/2 \leqslant \alpha \leqslant \pi. \end{cases} \tag{C.12}$$

Here $-1 \leqslant \xi \leqslant 1$, and the Jacobian

$$\frac{\mathrm{d}\cos(\theta_{12})}{\sqrt{1-\sin(\alpha)\cos(\theta_{12})}} = \begin{cases} \frac{(-\xi\tan(\alpha/2)+1)\mathrm{d}\xi}{\cos(\alpha/2)-\xi\sin(\alpha/2)} = \frac{\mathrm{d}\xi}{\cos(\alpha/2)}, & 0 \leqslant \alpha \leqslant \pi/2, \\ \frac{(-\xi\cot(\alpha/2)+1)\mathrm{d}\xi}{\sin(\alpha/2)-\xi\cos(\alpha/2)} = \frac{\mathrm{d}\xi}{\sin(\alpha/2)}, & \pi/2 \leqslant \alpha \leqslant \pi. \end{cases} \tag{C.13}$$

Finally the above integral (C.5) can be given in terms of the sum of two non-singular integrals

$$I = I_1 + I_2, \tag{C.14}$$

where

$$I_1 = \frac{1}{4}\int_0^\infty \mathrm{d}r r^4 \int_0^{\pi/2}\mathrm{d}\alpha \sin(\alpha)\sin(\alpha/2) \times \int_0^\pi \mathrm{d}\theta_1 \sin(\theta_1)\int_0^{2\pi}\mathrm{d}\phi_1\int_0^{2\pi}\mathrm{d}\psi\int_{-1}^1 \mathrm{d}\xi f(\mathbf{r}_1,\mathbf{r}_2),$$
$$I_2 = \frac{1}{4}\int_0^\infty \mathrm{d}r r^4 \int_{\pi/2}^{\pi}\mathrm{d}\alpha \sin(\alpha)\cos(\alpha/2) \times \int_0^\pi \mathrm{d}\theta_1 \sin(\theta_1)\int_0^{2\pi}\mathrm{d}\phi_1\int_0^{2\pi}\mathrm{d}\psi\int_{-1}^1 \mathrm{d}\xi f(\mathbf{r}_1,\mathbf{r}_2). \tag{C.15}$$

References

[1] Bleakney W 1932 *Phys. Rev.* **40** 496–501
[2] Saporoschenko M 1965 *J. Chem. Phys.* **42** 2760–4
[3] Allmendinger P, Deiglmayr J, Schullian O, Hoveler K, Agner J A, Schmutz H and Merkt F 2016 *ChemPhysChem* **17** 3596–608
[4] Hirschfelder J, Eyring H and Rosen N 1936 *J. Chem. Phys.* **4** 130–3
[5] Stevenson D and Hirschfelder J 1937 *J. Chem. Phys.* **5** 933–40
[6] Hirschfelder J O 1938 *J. Chem. Phys.* **6** 795–806
[7] Walsh J M, Moore R A and Matsen F A 1950 *J. Chem. Phys.* **17** 1070–2
[8] Christoffersen R E 1964 *J. Chem. Phys.* **41** 960–71
[9] Schwartz M E and Schaad L J 1967 *J. Chem. Phys.* **47** 5325–34
[10] Kawaoka K and Borkman R F 1971 *J. Chem. Phys.* **55** 4637–41
[11] Helm H, Galster U, Mistrík I, Müller U and Reichle R 2003 *Dissociative Recombination of Molecular Ions with Electrons* ed G Steven (Boston, MA: Springer) 275–88
[12] Strasser D, Levin J, Pedersen H B, Heber O, Wolf A, Schwalm D and Zajfman D 2001 *Phys. Rev.* A **65** 010702
[13] Oka T 1980 *Phys. Rev. Lett.* **45** 531–4
[14] Goto M, Geballe T R and Usuda T 2015 *Astrophys. J.* **806** 57
[15] Lam H A, Miller S, Joseph R D, Geballe T R, Trafton L M, Tennyson J and Ballester G E 1997 *Astrophys. J.* **474** L73–6
[16] Zuo T and Bandrauk A D 1995 *Phys. Rev.* A **51** R26–9
[17] Lötstedt E, Kato T and Yamanouchi K 2012 *Phys. Rev.* A **85** 053410
[18] Morrison J C, Bottcher C and Bottrell G 1991 *Theor. Chim. Acta.* **80** 245–55
[19] McKenna J, Sayler A M, Gaire B, Johnson N G, Carnes K D, Esry B D and Ben-Itzhak I 2009 *Phys. Rev. Lett.* **103** 103004
[20] McCarthy I E and Weigold E 1991 *Rep. Prog. Phys.* **54** 789–879
[21] Coplan M A, Moore J H and Doering J P 1994 *Rev. Mod. Phys.* **66** 985–1014
[22] Weigold E and McCarthy I E 1999 *Electron Momentum Spectroscopy* (New York: Kluwer)
[23] Chuluunbaatar O, Joulakian B B, Tsookhuu K and Vinitsky S I 2004 *J. Phys. B: At. Mol. Phys.* **37** 2607–16
[24] Staicu-Casagrande E M *et al* 2008 *J. Phys. B: At. Mol. Opt. Phys.* **41** 025204
[25] Naja A, Staicu-Casagrande E M, Lahmam-Bennani A, Nekkab M, Mezdari F, Joulakian B, Chuluunbaatar O and Madison D H 2007 *J. Phys. B: At. Mol. Opt. Phys.* **40** 3775–83
[26] Chuluunbaatar O, Gusev A A and Joulakian B B 2012 *J. Phys. B: At. Mol. Opt. Phys.* **45** 015205
[27] Bulychev A A, Chuluunbaatar O, Gusev A A and Joulakian B B 2013 *J. Phys. B: At. Mol. Opt. Phys.* **46** 185203
[28] Bolognesi P, Joulakian B, Bulychev A A, Chuluunbaatar O and Avaldi L 2014 *Phys. Rev.* A **89** 053405
[29] Chuluunbaatar O and Joulakian B 2010 *J. Phys. B: At. Mol. Opt. Phys.* **43** 155201
[30] Alwan O, Chuluunbaatar O, Assfeld X, Naja A and Joulakian B B 2014 *J. Phys. B: At. Mol. Opt. Phys.* **47** 225201
[31] Alwan O, Chuluunbaatar O, Assfeld X and Joulakian B B 2015 *J. Phys. B: At. Mol. Opt. Phys.* **48** 185203
[32] Iijima T, Bonham R A and Ando T 1963 *J. Phys. C: Solid State Phys.* **67** 1472–4
[33] Shulz M 1973 *J. Phys. B: At. Mol. Phys.* **6** 2580–92
[34] Lopez Vieyra J C, Turbiner A V and Medal-Cobaxin H 2011 *J. Phys. B: At. Mol. Opt. Phys.* **44** 195101
[35] Brenz F 1957 *Acta. Phys. Acad. Sci. Hung.* **6** 423
[36] Joulakian B, Hanssen J, Rivarola R and Motassim A 1996 *Phys. Rev.* A **54** 1473–9
[37] Pavanello M and Adamowicz L 2009 *J. Chem. Phys.* **130** 034104
[38] Medal-Cobaxin H, Alijah A and Turbiner A V 2008 *Collect. Czech. Chem. Commun.* **73** 1271–80
[39] Gusev A A, Chuluunbaatar O, Vinitsky S I and Abrashkevich A G 2014 *Comput. Phys. Commun.* **185** 2636–54